M23 Lab Report

Z0966990
L2 Mechanical Engineering

April 23, 2017

Abstract

In this report it is detailed how empirical, numerical and analytical approaches were used to investigate how stress and strain concentrations in plates vary around features. Strain gauges were used to measure the deformation of a plate under axial load with a circular hole stress raiser at the centre. From those measurements, the strain and stress concentrations in the plate were deduced. Those concentrations were compared to concentrations predicted by numerical simulations and analytical expressions. Numerical simulations were used to explore the relationship between the dimensions of shoulder fillets and the stress concentrations surrounding them. Parallels were then drawn between the circular hole and shoulder fillet stress raisers.

Nomenclature

Acronyms

BEM	Boundary element method
SE	Standard error

Background

E	Young's modulus of elasticity	GPa
H	Height of plate	mm
K_ϵ	True strain concentration factor	—
K_σ	True stress concentration factor	—
K_{σ_t}	Theoretical stress concentration factor	—
L	Length of plate	mm
S	Far-field stress	MPa
d	Height/diameter of plate feature	mm
r	Radius of plate feature	mm
ϵ_{nom}	Nominal strain	—
ϵ_{ww}	Normal strain in w-direction	—
ν	Poisson's ratio	—
σ_{max}	Maximum plate stress	MPa
σ_{nom}	Nominal stress	MPa
σ_{ww}	Normal stress in w-direction	MPa

Experiment

R^2	Coefficient of determinability	—
K_{ϵ_i}	Strain concentration factor at gauge i	—
K_{σ_i}	Stress concentration factor at gauge i	—
Δ	Gradient	—
α, β	Regression coefficients	—
ϵ_i	Strain at gauge i	—
σ_i	Stress at gauge i	MPa

1 Introduction

When designing structural components, engineers typically look to the most stressed point in that component to determine and specify failure criteria and factors of safety.

In simple systems, engineers can use intuition to identify candidates for possible points of failure. In more complex systems, such as components with smoothly varying features, more rigorous approaches to stress analysis are required. Experimentation, simulation and theory can all identify the most severely stressed point in a component.

In this report, finite width plates with either circular holes or shoulder fillets were analysed. Circular holes are a common feature present in many parts, allowing for fixtures such as screws and bolts to be used. Shoulder fillets are introduced to reduce the peak stress experienced by components with sharp internal corners.

2 Background

Plane stress problems are defined by their zero out of plane stress. The most common plane stress situations involve stresses resolved on the surface of plates.

On the plate boundary, the only non-zero principle stress component is tangential to the plate boundary. The relationship between the tangential stress and strain can be described using Hooke's law under axial load, given by

Hibbeler [1, p. 88]:

$$\sigma_{xx} = E\epsilon_{xx} \tag{1}$$

where x is the axial or tangential direction.

In the axial load case, shear strain is also zero. The Poisson effect can be used to determine Poisson's ratio if the axial and transverse strains are known. The following expression was also given by Hibbler [1, p. 106]:

$$\nu = -\frac{\epsilon_{yy}}{\epsilon_{xx}} = -\frac{\epsilon_{zz}}{\epsilon_{xx}} \tag{2}$$

2.1 Stress Concentrations

The stress concentration factor is a dimensionless quantity which describes how much greater the maximum principle stress in the feature is than the nominal—or average—stress in the part. Similarly, there also exists a strain concentration factor, which is a measure of relative deformation. According to Pilkey [2, p. 4]:

$$K_\sigma = \frac{\sigma_{max}}{\sigma_{nom}} \tag{3}$$

$$K_\epsilon = \frac{\epsilon_{max}}{\epsilon_{nom}} \tag{4}$$

For simple features—or stress raisers—such as the circular hole in Figure 1, the *theoretical* stress concentration factor K_{σ_t} can be determined analytically as described by Pilkey [2, pp. 180–181]:

$$K_{\sigma_t} = 3 \tag{5}$$

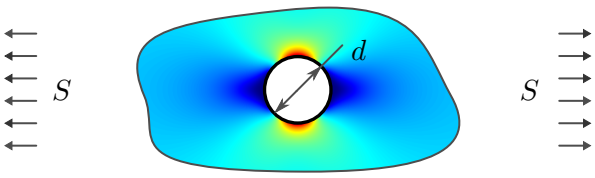

Figure 1: Circular hole stress concentrations.

Pilkey also offers equations to determine the local stress concentrations at any point in the plate; used to produce the contour plot in Figure 1. These reveal most stressed—red—points lie at the top and bottom of the hole.

However, when the plate has a finite width as illustrated in Figure 2, the problem becomes much harder to solve analytically. Howland [3] derived a more generalised stress concentration factor expression at the top and bottom of the hole, but not for the local stress concentrations throughout the rest of the plate:

$$K_{\sigma_t} = \frac{2 + (1 - d/H)^3}{1 - d/H} \tag{6}$$

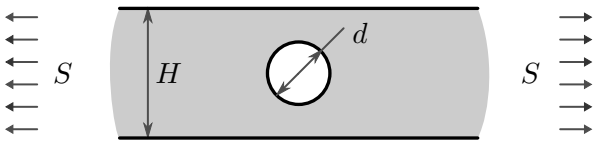

Figure 2: Finite width plate with circular hole.

Notice, in the limit as $H \to \infty$, (6) $\to$ (5).

For the shoulder fillets detailed in Figure 3, stress concentration factors are derived empirically rather than analytically. Pilkey [2, p. 151] provides a chart relating the ratios H/d and r/d to the stress concentration factor using data from multiple sources.

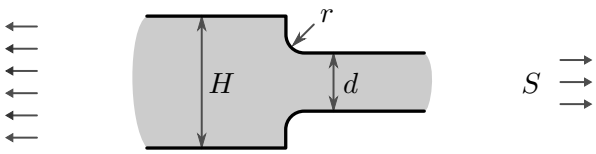

Figure 3: Finite width plate with shoulder fillets.

Therefore, to determine the location of the most stressed points, engineers must either measure or simulate the stress concentration factors in the plate, particularly for complex stress raisers.

One method of simulation is the Boundary Element Method—or BEM—a modern computational method which divides the complex

part into simpler elements using a mesh, resolving the stresses in each element to model the stress field.

3 Method

3.1 Circular Hole Stress Raiser

To investigate the properties of a circular hole stress raiser, strain gauges were used to measure the stress at several locations of interest in a plate with a circular hole placed under axial load. Figure 4 details the dimensions of the plate used in the experiment.

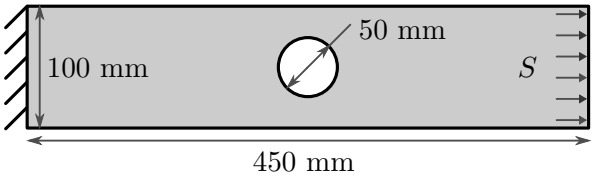

Figure 4: Dimensions of the experiment plate.

The apparatus included the plate, fixed at one end, with a thumb screw at the other to allow a range of loads to be applied. Strain gauges at the locations labelled in Figure 5 were connected to a PC such that the strain could be measured.

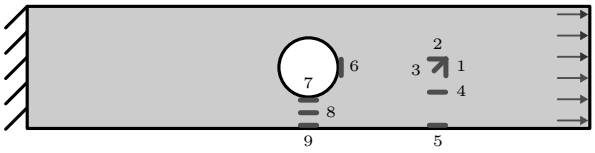

Figure 5: Positions of strain gauges on the experiment plate.

Gauge 2 was located away from the stress raiser, so the strain measured at gauge 2 would be close to the far-field strain. Therefore, it was taken as the nominal strain. The independent variable was the maximum strain measured across all the strain gauges, expected to be the strain measured at gauge 7 at the bottom of the hole. The strains measured at the other gauges were the dependent variables.

Three repeat readings were taken for five different maximum strains: 0, 200×10^{-6}, 400×10^{-6}, 600×10^{-6} and 800×10^{-6}. This avoided exceeding the 1000×10^{-6} limit for the apparatus, and gave sufficient repeat readings to determine errors.

Concept Analyst® BEM software was used to simulate the local stress concentrations in the plate to supplement the experimental results.

3.2 Shoulder Fillet Stress Raiser

Concept Analyst was also used to investigate how changing the geometry of a shoulder fillet stress raiser affected the stress concentration factor. Figure 6 details the the defining dimensions of the feature.

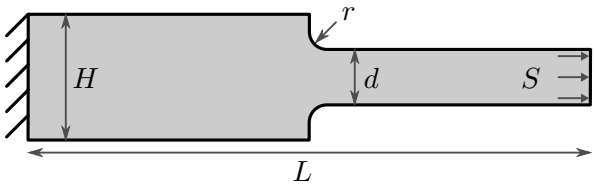

Figure 6: Dimensions of plate with shoulder fillets.

In practice, the plate detailed in Figure 6 was modelled with the feature height d kept constant at 100 mm. To investigate the effects of varying the ratio H/d, the simulations were run with H at 110 mm, 130 mm and 200 mm. For each H value, r/d was also varied by running the simulations with six different feature radii in the range 5 mm–10 mm.

L was initially chosen to be ten times greater than H, operating under the assumption that this was sufficiently long such that the plate behaved as if the far-field stress was applied an infinite distance away from the shoulder fillets. This allowed an infinitely long plate to be represented by a finite model.

The nominal far-field stress S was applied to the plate using a traction of magnitude 100 MPa. The exact magnitude of this load was not important as the stresses were later normalised by the chosen far-field stress to find the stress concentration factors.

To investigate how the stress concentration factor changes in a plate with a finite length, L/H was then reduced from 5 to 0.5, corresponding to ten lengths in the range 1000 mm–50 mm. H was kept constant at 200 mm, d at 100 mm and r at 10 mm.

4 Results

4.1 Circular Hole Stress Raiser

Figure 7 details the strains measured at each gauge, plotted against the nominal strain at gauge 2.

Least squares regression lines were fitted to the data for each strain gauge, including repeats. Taking gradients of the line for each strain gauge yielded the local stress concentration factors in Table 1. When the nominal strain is zero, all other strains are zero, leading to the following:

$$\Delta = \frac{\epsilon_i - 0}{\epsilon_{nom} - 0} = \frac{\epsilon_i}{\epsilon_{nom}} = K_{\epsilon_i}$$

Table 1: Local strain concentration factors measured around circular hole.

K_{ϵ_1}	-0.314 ± 0.016
K_{ϵ_2}	1.000 ± 0.000
K_{ϵ_3}	0.348 ± 0.010
K_{ϵ_4}	1.043 ± 0.032
K_{ϵ_5}	1.001 ± 0.033
K_{ϵ_6}	-1.559 ± 0.040
K_{ϵ_7}	4.564 ± 0.103
K_{ϵ_8}	1.714 ± 0.045
K_{ϵ_9}	0.760 ± 0.017

$K_{\epsilon_i} \pm 95\%$ confidence

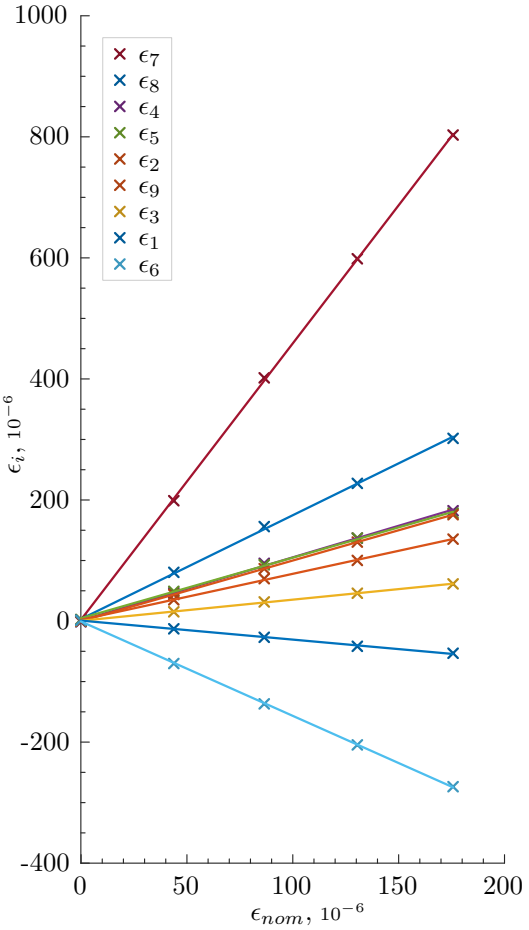

Figure 7: Strains measured around circular hole, plotted against nominal strain.

4.2 Shoulder Fillet Stress Raiser

The contour plots for the stress concentrations in the extremes of the shoulder fillet geometry are displayed in Figure 8 on the following page.

The maximum stresses in each contour plot were divided by the far-field stress to find the stress concentration factor for each combination of H/d and r/d. These are recorded in Figure 9 on the next page, plotting the stress concentration factor against r/d for each H/d on $\log_{10}$–$\log_{10}$ scale.

Least squares regression lines were fitted to the data in log-space, indicating a power law

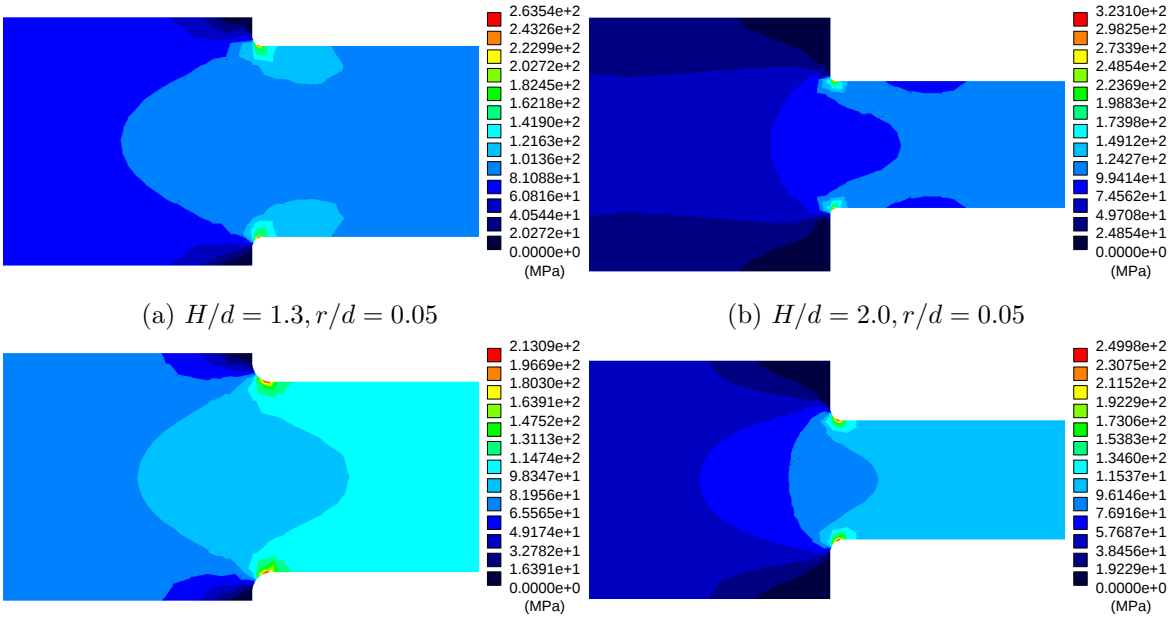

(a) $H/d = 1.3, r/d = 0.05$ (b) $H/d = 2.0, r/d = 0.05$

(c) $H/d = 1.3, r/d = 0.10$ (d) $H/d = 2.0, r/d = 0.10$

Figure 8: Stress concentrations simulated for shoulder fillets with different H/d and r/d.

relationship of the following form:

$$K_{\sigma_t} = \alpha \left(\frac{r}{d}\right)^{\beta} \tag{7}$$

Figure 10 records the stress concentration factor of shoulder fillets as the length of the plate was reduced from effectively infinite to finite values.

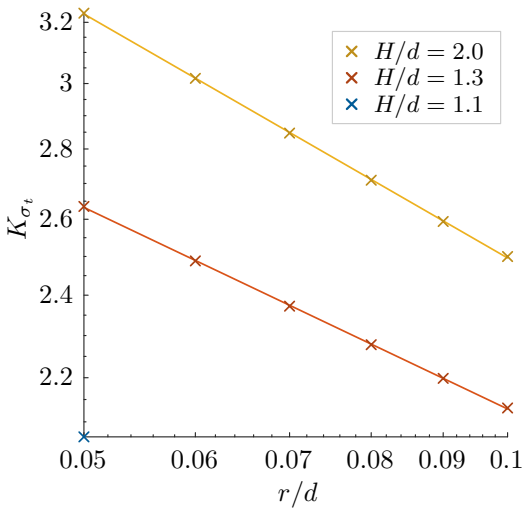

Figure 9: Stress concentration factors of shoulder fillets with different H/d and r/d. Scale: $\log_{10}$–$\log_{10}$

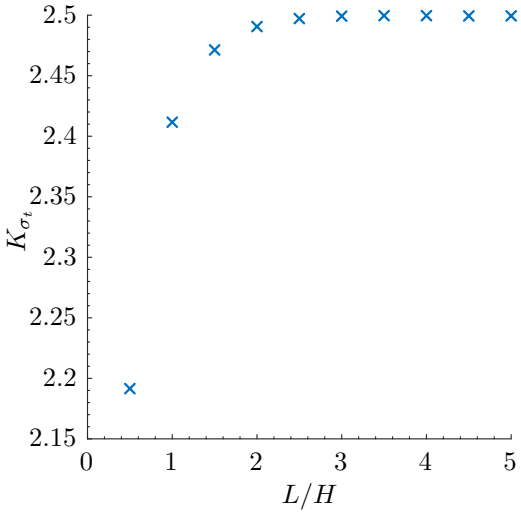

Figure 10: Stress concentration factors of shoulder fillets with different L/H.

5 Discussion

5.1 Circular Hole Stress Raiser

Gauge 2 measured the nominal strain under axial load and gauge 1 is perpendicular at the same location, suggesting the relationship between the two strains can be described by the Poisson effect. Substituting ϵ_{nom} and ϵ_1 into (2) yields the following:

$$\nu = -\frac{\epsilon_1}{\epsilon_{nom}} = -K_{\epsilon_1}$$

Therefore, Poisson's ratio for the plate used in the experiment can be obtained from Table 1 on page 4, which suggests a 95% confidence interval for ν: 0.314 ± 0.016. Assuming the plate was made from machined aluminium, a sensible alloy choice would have been 6086. According to the American Society for Metals [4], Aluminium 6086 and similar alloys have a Poisson's ratio of 0.33 at room temperature, which is contained in the 95% confidence interval for Poisson's ratio estimated empirically. At the 5% level of significance the measured Poisson's ratio did not differ from the true Poisson's ratio of the material.

Gauges 5, 6, 7 and 9 were located on the plate boundary, so the axial load form of Hooke's law applied. Substituting (1) into (3) yields the expression for strain concentration factor given in (4):

$$K_\sigma = \frac{\sigma_{max}}{\sigma_{nom}} = \frac{\cancel{E}\epsilon_{max}}{\cancel{E}\epsilon_{nom}} = K_\epsilon \qquad (8)$$

From (8), it can be deduced that the local stress concentration factors at the locations of these gauges were the same as the local strain concentration factors calculated in Table 1. These are displayed in Table 2.

The contour plot from the simulation in Figure 11 reveals the maximum stress coincided with the location of gauge 7. Therefore, K_{σ_7} must be an empirical measurement of the overall stress concentration factor in the plate.

Table 2: Local stress concentration factors measured around circular hole.

K_{σ_5}	1.001 ± 0.033
K_{σ_6}	-1.559 ± 0.040
K_{σ_7}	4.564 ± 0.103
K_{σ_9}	0.760 ± 0.017

$K_{\sigma_i} \pm 95\%$ confidence

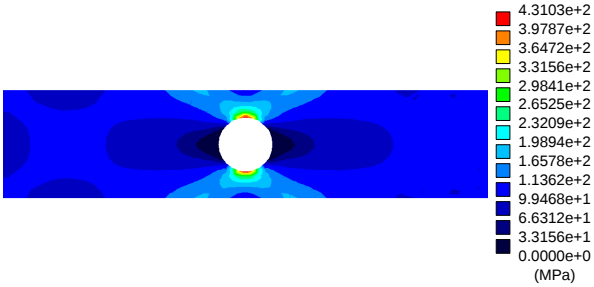

Figure 11: Stress concentrations simulated around circular hole.

The maximum stress recorded in Figure 11 was 4.310 MPa and the far-field stress applied was 100 MPa. Applying (3) yielded a numerical prediction of the stress concentration factor. Another prediction was obtained by plugging the dimensions of the plate in Figure 4 into the analytical equation, (6). These are compared to the empirical value obtained in Table 3.

Table 3: Comparison of approaches.

Analytical	K_{σ_t}	4.250
Numerical	K_{σ_t}	4.310
Empirical	K_{σ_7}	4.564 ± 0.103

$K_{\sigma_7} \pm 95\%$ confidence

The stress concentration factors predicted by (6) and the Concept Analyst simulation are similar to—but do not lie within—the 95% confidence interval for the stress concentration factor found empirically. At the 5% level of significance, the stress concentration factor in the plate was not what the theoretical values suggested after accounting for random errors.

It is unlikely the empirical value obtained was more accurate than prior experiments which were the basis for the theoretical values above. The systematic errors—or inaccuracies—in this experiment can be explained by three main factors: inhomogeneity in the plate, calibration of the strain gauges and different measurements of the far field stress.

Equation (1)—Hooke's law under axial load—only applies to members homogeneous in the axial direction. However, the plate may not have a constant thickness, particularly at the machined edges. Although instructions warn against tensioning the plate beyond 1000×10^{-6} strain to avoid plastic deformation, previous groups may have over-tensioned the plate. The most stressed region at the location of gauge 7 would be the first to yield and consequently the thinnest region. The thinnest regions are subjected to greater stress concentrations which the analytical model and BEM do not account for. The argument also applies to the width of the plate.

Strain gauges increase in resistance as strain increases. The constant of proportionality by which they change is calibrated upon installation, but over time may vary due to temperature changes, break down of adhesives and degradation of the strain sensitive resistor. If the constant of proportionality for gauge 7 was greater than for gauge 2, the strain concentration factor would be overestimated.

The nominal strain gauge 2 was located half way between the hole and the boundary where the far field stress was applied. The contour plot in Figure 11 suggests this would lead to an underestimation of the far-field stress, as stresses get smaller in the middle of the plate close to the stress raiser. Equation (4) suggests K_ϵ and ϵ_{nom} are inversely proportional, so an underestimation in far-field strain would lead to an overestimation in the strain and stress concentration factors.

In practice, the factor of safety used to design parts can be increased to account for the error in predictions of stress concentration factors.

5.2 Shoulder Fillet Stress Raiser

The contour plots in Figure 8 on page 5 reveal the most stressed regions of the shoulder fillets and the points of failure in the event of yield were on the fillet radii close to where the boundary and the far-field were tangential, for all ratios H/d and r/d. This is consistent with the most stressed regions of the circular hole stress raiser, detailed in Figures 1 and 11, which were located on the top and bottom of the hole where the far-field was tangential to the boundary.

In both cases these were the points where the force lines navigating the stress raiser were most deflected and consequently most concentrated.

Conversely, the sharp corner on the outside of the feature radii experienced zero stress. This is justified because there is no continuous path for the force lines into and out of the the corner, so the corner bears neither load nor stress.

The stress concentration factor decreased as the ratio of feature radius to minor plate width—r/d—increased, according to an inverse power law. This is evidenced by the negative gradient of the best fit lines in Figure 9. Table 4 lists coefficients of the power model with which the lines were fitted.

Table 4: Fitted power models for shoulder fillets plotted on Figure 9. of the form $K_{\sigma_t} = \alpha(r/d)^\beta$

H/d	α	β	R^2
1.1†	1.000 ± 0.000	-0.2424	—
1.3	1.051 ± 0.013	-0.3065 ± 0.0046	0.999 88
2.0	1.062 ± 0.014	-0.3711 ± 0.0052	0.999 90

† Insufficient data to effectively determine model.
$\alpha, \beta \pm 95\%$ confidence

From inspecting the closeness of the data to the model, and noting how near the coeffi-

cients of determinability are to one, it can be deduced the models were a good fit to the data when H/d was 1.3 or 2.0. Formally, the overall p-values from the minimised χ^2 regression test statistic were 1.76×10^{-7} and 2.18×10^{-7} respectively; at the 5% significance level, the data was consistent with the model. With only a single data-point, it was impossible to determine whether data fitted any model when H/d was 1.1.

The β coefficients in the range -0.4 to -0.3, suggested increasing the radius had less of an effect on the stress concentration factor as the magnitude of radius increased, leading to diminishing reductions in stress concentrations. However the range of the the ratio r/d is bounded between zero and the height of the step from the minor plate width L to the major plate width H as follows:

$$\begin{cases} r > 0 \\ H \geq d + 2r \end{cases} \Rightarrow 0 < \frac{r}{d} \leq \frac{1}{2}\left(\frac{H}{d} - 1\right) \tag{9}$$

Therefore, assuming the power law continues to hold, there exists a minimum stress concentration factor in plate when the radius is at a maximum—the distance from the major plate width to the minor plate width. In Figure 12, the lines in Figure 9 on page 5 have been extrapolated in linear-space to the limits of r/d to demonstrate this.

Figure 12 also illustrates the stress concentration factor becomes unbounded as the radius goes to zero. In practice, its impossible to manufacture an internal corner without a small radius. Nonetheless, including a radius feature in the design of shoulder features is critical to avoiding large stress concentrations.

With regards to the change in plate width across the stress raiser, the effect of increasing H/d can be seen too. The plates with a greater ratio H/d had greater stress concentration factors for the same r/d values. Consequently, to maintain the same stress concentration factor for a greater H/d ratio requires using a larger radius for the shoulder fillet.

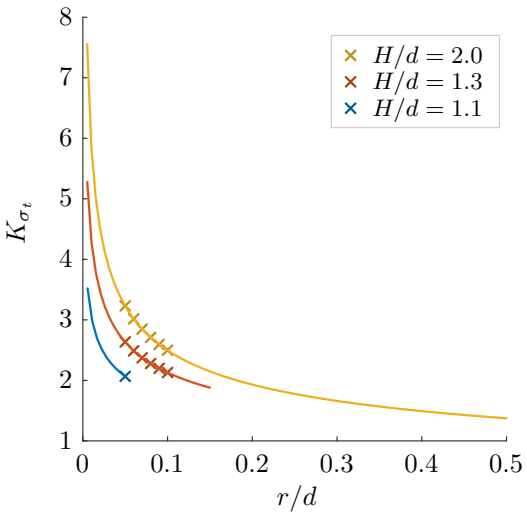

Figure 12: Extrapolated stress concentration factors of shoulder fillets for different r/d and H/d.

In industry, engineers use more complete charts of a similar form to the one in Figure 12 to specify the geometry of the part they are designing. It is more likely the ratio H/d would be the driving dimension of a shoulder fillet feature—on a shaft with a change in diameter for example. The radius can then be specified to meet the stress concentration factor requirement after considering the loads and failure criteria of the material. An example of such a chart is referenced in Section 2.1 and referenced again here [2, p. 151].

These charts are only valid when the plate is sufficiently long with respect to it's width. The plate in Figure 8d on page 5 was modelled with H/d at 2.0, r/d at 0.10, L/d at 10 and yielded a stress concentration factor of 2.4998.

Figure 10 on page 5 suggests the stress concentration factor remained largely constant when $L/H > 3$, accounting for numerical noise.

When $L/H > 3$, the mean for K_{σ_t} was 2.4994 with a one-tailed 95% lower confidence limit of

2.4992. The mean included included data when L/H was 6, 7, 8, 9 and 10. Table 5 lists the confidence limits for all values tested and confirms 3 was the largest L/H ratio for which the reduction in stress concentration was significant at the 5% level.

Table 5: 95% confidence limits for mean K_{σ_t} in shoulder fillets calculated from data when $L/H > x$, compared with K_{σ_t} measured when $L/H = x$.

L/H	K_{σ_t}		Limit − Actual
	Limit†	Actual	
0.5	2.479 01	2.191 50	2.88×10^{-1}
1.0	2.492 47	2.411 60	8.09×10^{-2}
1.5	2.497 14	2.471 30	2.58×10^{-2}
2.0	2.498 81	2.490 60	8.21×10^{-3}
2.5	2.499 25	2.497 20	2.05×10^{-3}
3.0	2.499 25	2.499 20	5.48×10^{-5}
3.5	2.499 21	2.499 60	-3.86×10^{-4}
4.0	2.499 16	2.499 60	-4.37×10^{-4}
4.5	2.499 11	2.499 40	-2.87×10^{-4}
5.0	2.499 03	2.499 40	-3.66×10^{-4}

† mean − 95% confidence

Consequently, the model in Figure 12 on the preceding page is not a good fit when $L/H \leq 3$. Similar length constraints will apply for different H/d and r/d ratios to the respective 2.0 and 0.10 values chosen for this analysis.

6 Conclusions

For finite width plates with circular hole and shoulder fillet stress raisers, the most stressed points both lie on the plate boundary at the top or bottom of the hole or on the inside of the shoulder fillet, where the force lines through the part are most concentrated.

Simulations can be used to find stress concentration factors which are close to the true stress concentration factors in the material. However, small errors in measurements can lead to lead to inaccuracies in predictions. This reaffirms the importance of factors of safety in the design of structural parts.

Simulations outlined the relationship between shoulder fillet radii and stress concentration factors in plates, suggesting an inverse power law. Extrapolating the power law revealed small fillet radii lead to very large stress concentration factors and the minimum stress concentration factor is achieved by maximising the fillet radii.

The same simulations also suggested increasing the ratio of the major plate width over the minor plate width leads to greater stress concentration factors for the same fillet radii. Engineers can use charts and tables to specify the required fillet radii for a particular part to meet loading requirements.

The models used and relationships derived in this report apply to plates of a sufficient length. For plates with shoulder fillets, when the ratio of the length over the width of plate is 3 or less, alternative models must be devised.

References

[1] R. C. Hibbeler, *Mechanics of Materials*, 10th ed. Pearson Higher Education, 2017, pp. 88–106.

[2] W. D. Pilkey and D. F. Pilkey, *Peterson's stress concentration factors*, 3rd ed. John Wiley & Sons, 2008, pp. 4–181.

[3] R. Howland, "On the stresses in the neighbourhood of a circular hole in a strip under tension", *Philosophical Transactions of the Royal Society of London*, vol. 229, pp. 49–86, 1930.

[4] ASM International, *Properties and Selection: Nonferrous Alloys and Special-Purpose Materials*, 10th ed. American Society of Metals, 1990, vol. 2 of Metals Handbook.